IET Power Electronics

Special issue Call for Papers

Be Seen. Be Cited. Submit your work to a new IET special issue
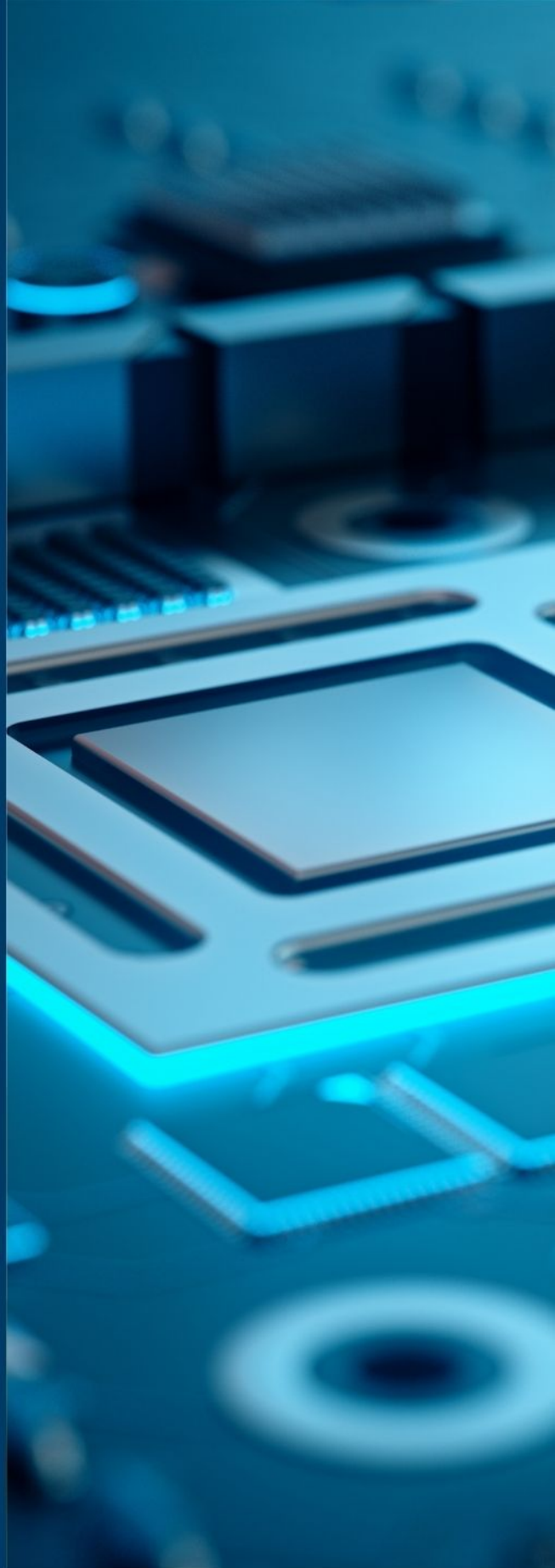
Connect with researchers and experts in your field and share knowledge.

Be part of the latest research trends, faster.

Read more

IET Power Electronics

ORIGINAL RESEARCH PAPER

Design and development of a new three-phase AC-DC single-stage wind energy conversion system

Kumar Abhishek Singh | **Kalpana Chaudhary** [ID]

Department of Electrical Engineering, Indian
Institute of Technology (BHU), Varanasi, India

Correspondence
Kumar Abhishek Singh, Department of Electrical
Engineering, Indian Institute of Technology (BHU),
Varanasi-221005, India.
Email: kabhisheksingh.rs.eee17@itbhu.ac.in

Abstract
The prevalent use of the diode bridge rectifier in three phase wind energy conversion systems decreases the efficiency of the power generation. In standalone wind energy generation, bridgeless converters can address this problem by eliminating the front-end diode bridge rectifier. This work presents a novel single-stage three-phase bridgeless AC to DC cùk converter for wind energy conversion systems. The proposed converter is designed to work in discontinuous inductor current mode because of its inherent power factor correction and less harmonic distortion. Using body-diodes of the MOSFETs per phase component reduction is also done in this converter. A unique maximum power point tracking technique is developed for this converter using three-phase voltages and currents, instead of the DC link states. A wind energy emulation system using a DC motor and self excited induction generator is used to test the laboratory prototype of the proposed converter.

1 | INTRODUCTION

Non-conventional energy sources are the only viable option to alleviate the increasing energy demand with sustainable development [1]. Compared to other renewable energy sources, wind energy is economical and more suitable for rural standalone application [2]. In standalone WECS, a DBR is conventionally used for AC to DC power conversion, followed by a DC–DC converter for MPPT. The front-end DBR decreases the conversion efficiency due to conduction losses; it is reported in [3] that the elimination of input diode bridge can increase the efficiency by around 2% . Thus, to increase efficiency of the WECS bridgeless AC–DC converters are optimal [4–12]. The active power quality improvement by eliminating the DBR has already been successfully achieved using a single-phase bridgeless buck [12], boost [9, 13], cùk [5, 6, 8, 11], single-ended primary-inductor converter (SEPIC) [4, 14] converters. A single-phase bridgeless AC-DC converter with three-port output has been reported in [15].

The currently available bridgeless AC–DC converters are mostly designed for single-phase conversion systems. These converters increase the efficiency of the system by eliminating the front-end DBR[4, 5, 10, 12] but are lacking in

system performance, which can be achieved using three-phase systems. Three-phase power generation using permanent magnet synchronous generator or self-excited induction generator (SEIG) in a standalone system has a lesser cost and higher efficiency than a single-phase power generator [16] maximum power point tracking (MPPT) techniques for WECS are widely used by sensing torque and turbine speed or by sensing the DC current and voltages obtained after rectification [2, 17–19]. In the proposed system there is no intermediate DC link after the three-phase generator; thus, a new MPPT technique is implemented.

Bridgeless boost converters exhibit excellent PFC, efficiency, ease of control and low cost. However, the lack of a wide range of voltage control makes them unsuitable for MPPT across the available range of wind power. To alleviate this problem, a buck stage is used in [20, 21], which leads to decrease in system efficiency.

In this paper, a novel single-stage three-phase bridgeless cùk converter is proposed, the converter is designed with the input inductors working in the DICM, while in the output inductors in continuous inductor current mode (CICM). This improves power quality in the source side and has a low DC voltage ripple
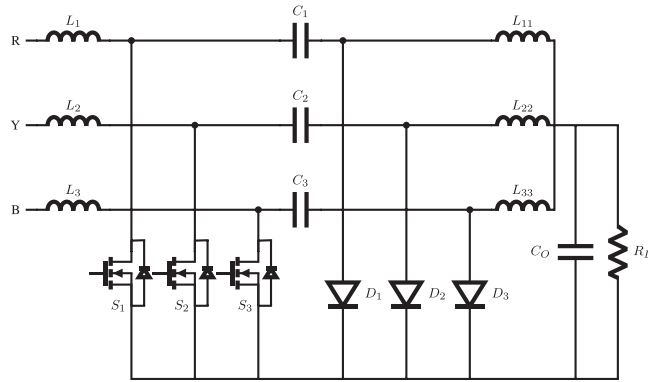
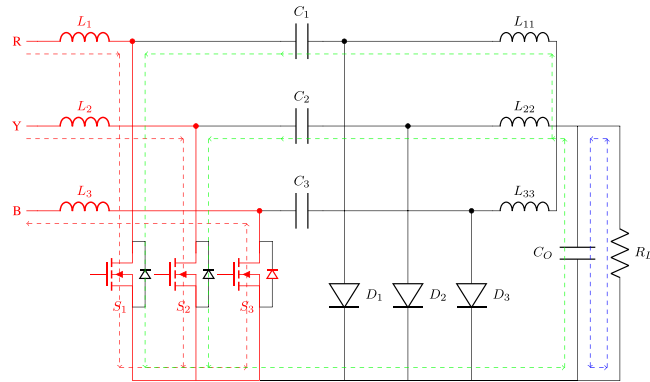**FIGURE 1** Circuit topology of the proposed converter

FIGURE 3 Current directions with switches in "OFF" state and input inductors energized (mode-2)

FIGURE 2 Current directions with switches in "ON" state (mode-1)
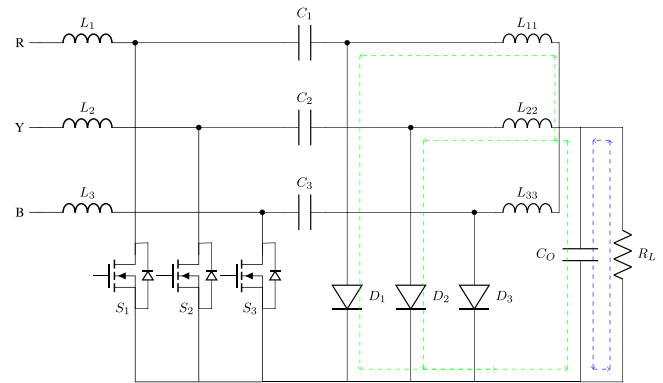
FIGURE 4 Current directions with switches in "OFF" state with input inductors de-energized (mode-3)

in the output. A DC motor is used for emulating wind turbines, which is coupled with a SEIG.

This paper is organized as follows: The circuit description, operation, design, and analysis are collated in Section 2. The implementation technique of the wind turbine emulation is presented in Section 3. The discussion on simulated results is done in Section 4. Hardware results are given with a discussion in Section 5. The conclusion regarding this work is drawn in Section 6.

2 | THREE PHASE BRIDGELESS CÙK CONVERTER

2.1 | Circuit description

The proposed three-phase bridgeless cùk converter is designed to operate in a wide range of input voltage and frequency fluctuations and has the capability to maintain the desired output voltage. The wind energy is highly stochastic; thus, the wide-range voltage tracking capability of this converter makes it ideal for MPPT in WECS.

The Bridgeless cùk and SEPIC converters are generally used with two diodes per phase in typical configurations. In the proposed topology the number of diodes per phase is reduced to one by using the body diodes of the MOSFETs as shown in Figure 1
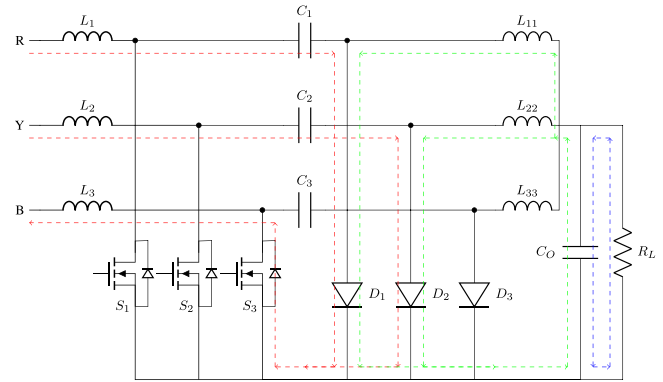
This converter is designed to operate at 100 kHz and discontinuous input inductor current; thus has small inductance requirement, which leads to lower weight and size. Conventional bridgeless converters require DBR to be connected before the input inductors [7, 8, 11]. The low inductance requirement and

TABLE 1 DESIGN PARAMETERS

Parameter	Value
Input rms voltage(V_{in})	415 V
Output power(P_o)	500 W
Output voltage(V_o)	250 V
Opearting frequency (f)	10^5

TABLE 2 DESIGNED CONVERTER PARAMETERS

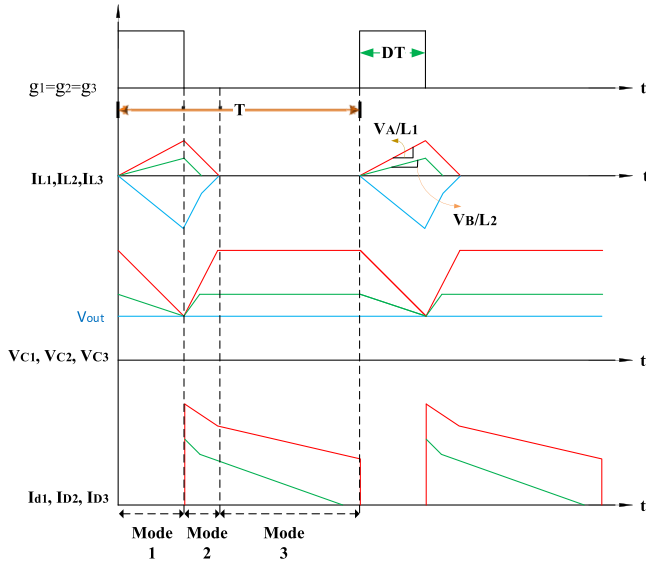| Parameters	Value
Input inductor (Li)	47 μH
capacitor (C)	1 μF
Output inductor (Lo)	560 μH
Output capacitor (Co)	1000 μF

FIGURE 5 Key waveforms of the proposed converter

absence of the input side DBR makes it possible to use the leakage inductance of the generator to be used as the input inductors in the proposed converter.

2.2 | Circuit operation

It is shown in Figure 1 that the input to the converter is a three-phase voltage source. The input inductors are L_1, L_2 and L_3. These input inductors are being switched by three MOSFETs namely S_1, S_2 and S_3.

As the MOSFETs are switched to "ON" state, the input inductors start to get energized, and capacitors C_1, C_2 and C_3 begin discharging into the output capacitor C_o and load R_L through the output inductors L_{11}, L_{22} and L_{33}. The operation of the proposed converter can be broadly divided into three parts as mode-1, mode-2 and mode-3, discussed as follows. The operation of the converter is represented in the Figure 5.

2.2.1 | Mode-1

In this mode, all the switches are in "ON" state, as shown in Figure 2. The input inductors start to charge according to the applied phase voltage across them. The inductors with positive voltage start to build up a positive current, while the inductor with a negative potential difference starts to build negative current across them. The capacitors having a higher voltage than the output capacitor starts to discharge through the switches and the output inductors. Figure 2 shows the modes of operation for a particular condition in which voltages at terminal R and Y are positive with terminal R at a higher voltage. While the terminal B is at a negative voltage.

2.2.2 | Mode-2

In mode-2, switches S_1, S_2 and S_3 are simultaneously switched to "OFF" state; this marks the end of Mode-1. Figure 3 shows an instance of Mode-2, where phase R and Y have positive, while phase B has negative voltage. The inductors with positive current(L_1 and L_2) and negative current-carrying inductor (L_3) discharges in capacitors (C_1 and C_2) through diodes (D_1 and D_2) and body-diode of S_3. The voltage of capacitors(C_1 and C_2) becomes higher than the output capacitor (C_o). The output inductors (L_{11} and L_{22}) discharges in the output capacitor(C_o) through diodes (D_1 and D_2). The capacitor (C_3), diode (D_3) and output inductor (L_{33}) carry no current as long as the polarity of phase B is negative. The active components change with polarity of source voltage.

2.2.3 | Mode-3

The input inductors are fully discharged in this mode. The increased voltage across the capacitors is sustained as long as the switches are in "OFF" state. Only the output inductors and the diodes are conducting in this mode. The stored energy in the output inductor is being transferred to the output capacitor. The switching of the MOSFETs to "ON" state marks the end of this mode.

The sinusoidally varying voltages across three-phase supply ensure equal current sharing by the switches and diodes and thus increases the reliability of this converter.

2.3 | Converter design

For designing the circuit parameters, it is mathematically convenient to change the system in per phase quantity for doing the calculations as we do with three-phase electrical machines. The design parameters are given in Table 1. The average voltage can be calculated using these parameters:

$$\text{Per phase voltage } (V_{pp}) \approx 240 \text{ V.}$$

$$\text{Maximum Phase Voltage } (V_m) \approx 340 \text{ V.}$$

$$\text{Average Voltage } (V_{in}) = \frac{\sqrt{2}V_{pp}}{\pi} = 108 \text{ V,}$$

$$\text{also Duty Cycle } (D) = \frac{V_o}{V_o + V_{in}} = 0.698.$$

For efficient DICM operation, the duty cycle is taken as 0.6. For three phase system this duty becomes $0.6/3 = 0.2$.

For DICM in L_1,

Current Ripple $(\Delta I) = 2 \times$ average current.

$$\Delta I = \frac{2P_o}{3V_{in}} = 3.086 \text{ A} \qquad (1)$$
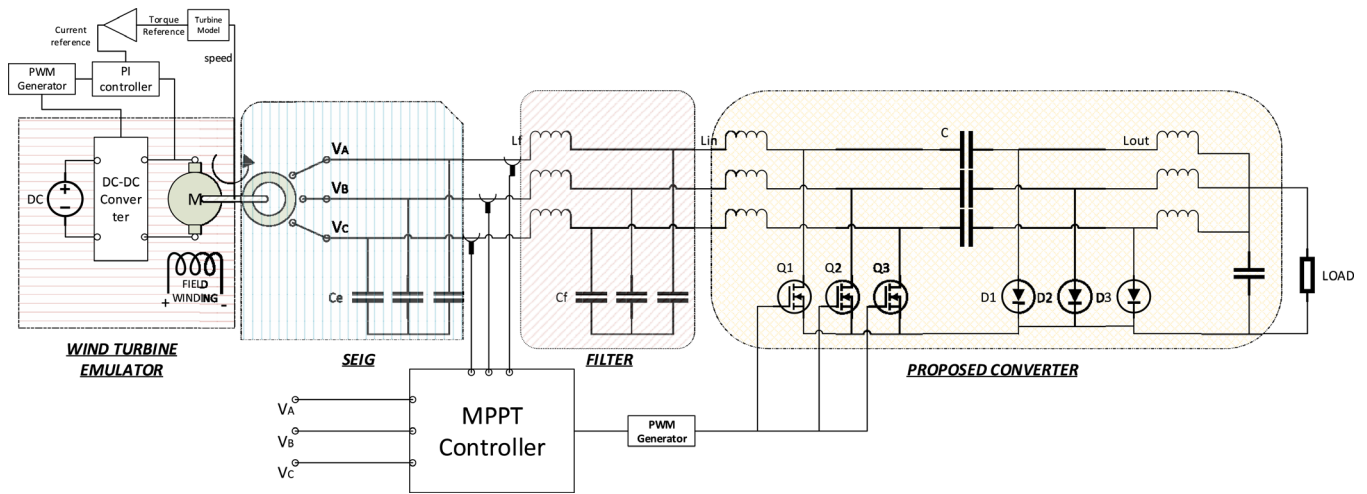
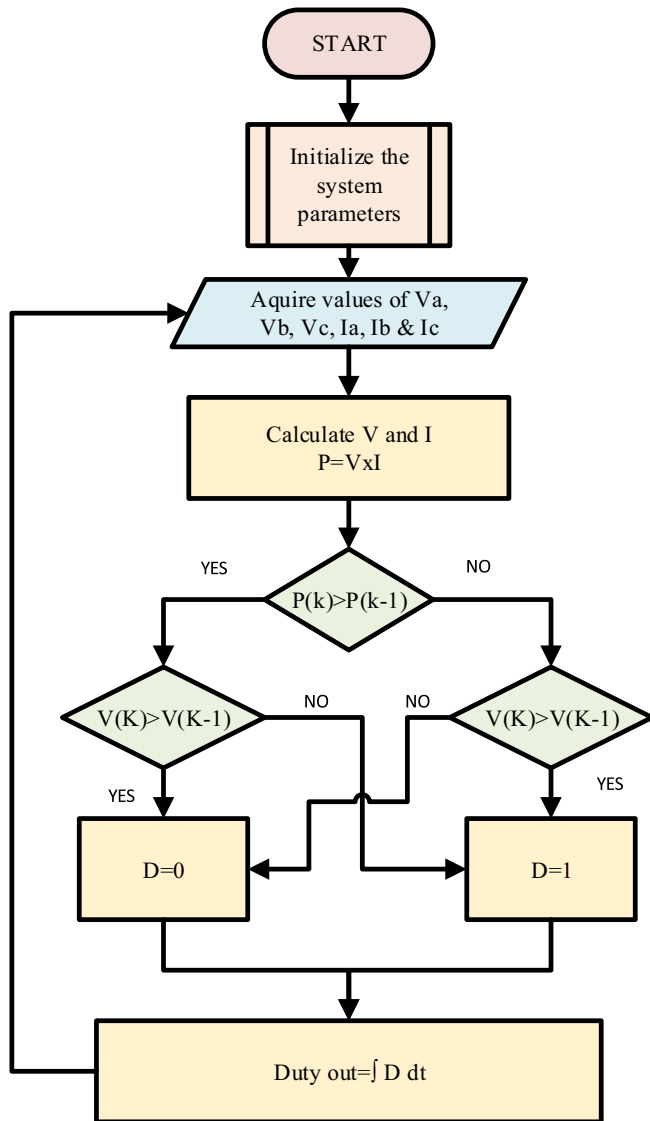**FIGURE 6** The schematic diagram of wind energy emulation and conversion system

FIGURE 7 Flowchart of MPPT technique

TABLE 3 TURBINE PARAMETERS

Parameters	Values
Blade sweep area	2 m^2
Air density	1.225 kg/m^3
Wind speed	8–12 m/s
Torque constant of DC motor	1.07 Nm/A
Proportional constant (K_p)	0.3
Integral constant (K_i)	6

therefore, input inductor

$$L_i = \frac{V_m D T_s}{\Delta I} = 219 \,\mu\text{H} \tag{2}$$

For Deep DICM operation of converter the value of input inductor is taken as 47 μH.

$$(Ka)_{\text{critical}} = \frac{1}{2(1 + M)^2} \tag{3}$$

$$= \frac{1}{2[(Vo/Vm) + 1]^2} = 0.33159 \tag{4}$$

As, $Ka < (Ka)_{\text{critical}}$

Hence, Ka is taken as 0.25. After determining Ka, the equivalent Inductance of the circuit can be calculated by using:

$$L_{\text{eq}} = \frac{RoTsKa}{2} = \frac{250^2 \times 10^{-5} \times 0.25}{2 \times 500} \tag{5}$$

$$= 156.25\mu\text{H} \tag{6}$$

Hence, the value of output inductor can be calculated as:

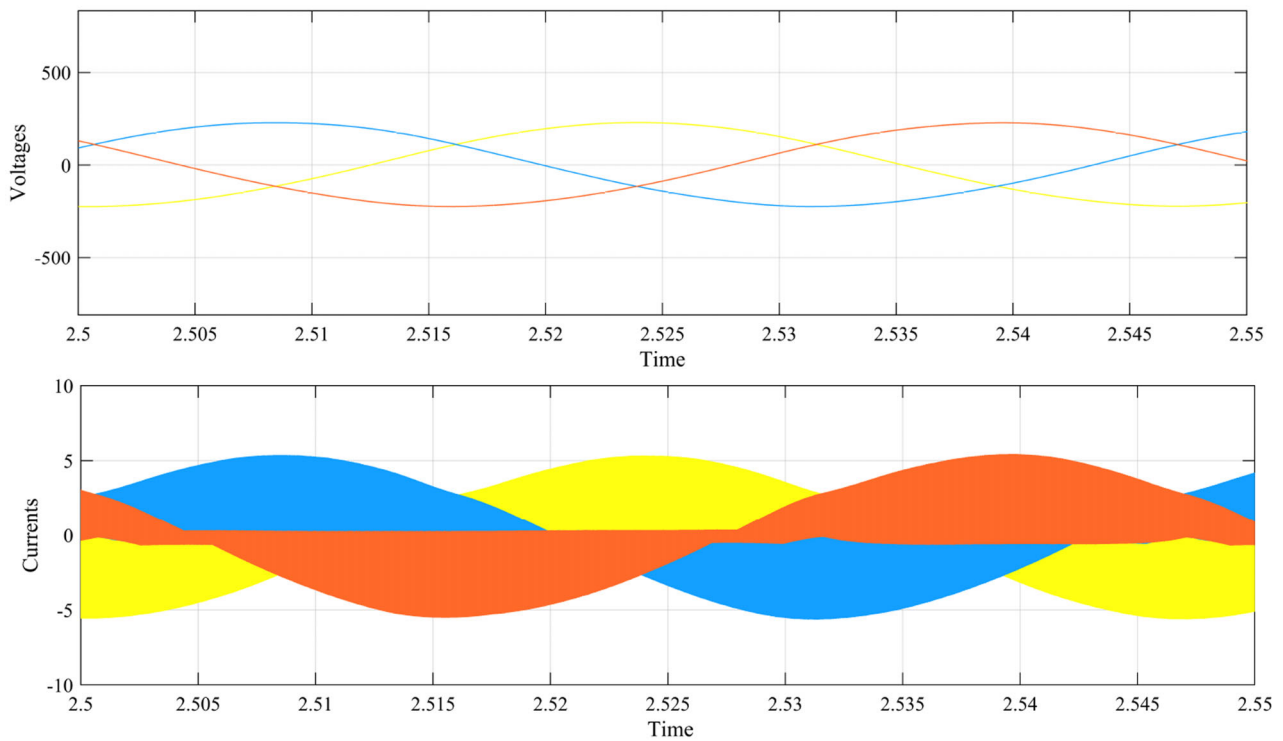$$Lo = \frac{Li \times L_{\text{eq}}}{Leq - Li} = 67\mu\text{H} \tag{7}$$
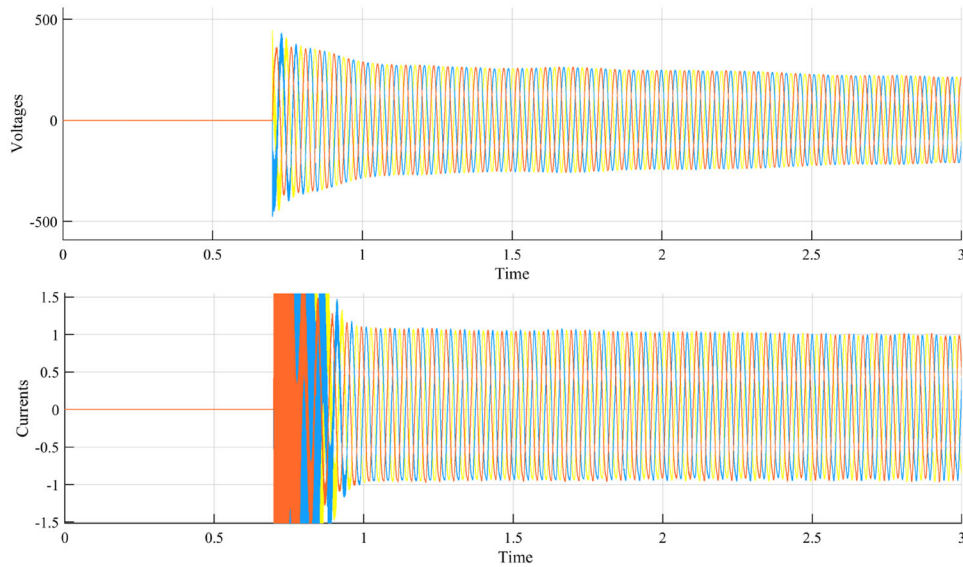
FIGURE 8   Input current and voltage waveform

FIGURE 9   Voltage and current waveform from source

As the output inductor is intended to be in CICM, thus an inductor value of 560 μH is chosen in this work.

The value of the capacitor is calculated by using the filter equation. Taking the frequency at the logarithmic mean of 10^5 and 50 Mz. ($F_s = 2250$ Mz), capacitance C is calculated as:

$$C = \frac{1}{(2 \times \pi \times 2250)^2 (47 + 560)10^{-6}} = 8.3457 \mu F \quad (8)$$

The capacitor value for $Fs = 5000$, which is also a good selection for filter comes around 2.2 μF. Thus taking the amount of leakage current into account, the value of capacitors is chosen at the commercially available 1 μF. The designed parameters of the circuit are summarized in Table 2.

The Value of Output capacitor is taken as 1000 μF as it is high enough to bring down the voltage ripples to less than 2% of the output voltage at rated load.
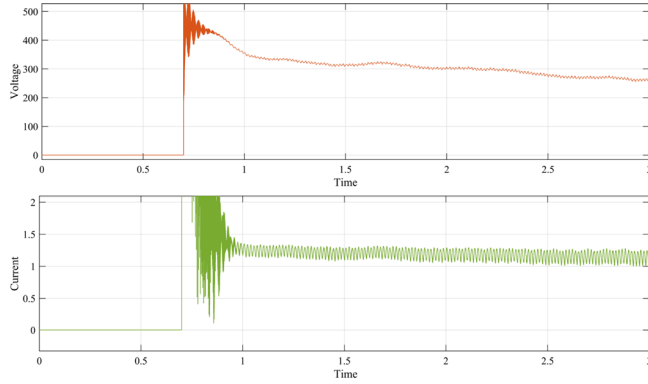
FIGURE 10 Calculated voltage and current maxima

2.4 | Converter analysis

The designing is done in order to keep the input inductor in deep DICM. Thus converter analysis is also done with the same consideration. For finding the converter voltage gain Vo/V_{in}, its necessary to find the voltages across each input inductor.

$$VR = Vm \sin(\omega t) \tag{9}$$

$$VY = Vm \sin(\omega t + 2\pi/3) \tag{10}$$

$$VB = Vm \sin(\omega t - 2\pi/3) \tag{11}$$

On adding the squares of the above voltages we get;

$$VR^2 + VY^2 + VB^2 = \frac{3}{2}Vm^2 \tag{12}$$

Thus, total energy absorbed per phase in DT time is:

$$dE = \text{Voltage} \times (\text{Current at time } t) \times dt \tag{13}$$

$$= VL \times \frac{VLt}{L}dt \tag{14}$$

Thus, total energy absorbed per phase in DT time is:

$$\Delta E = \int_0^{DT} \frac{VL^2 t}{L}dt \tag{15}$$

$$= \frac{VL^2 D^2 T^2}{2L} \tag{16}$$

The total energy absorbed can be calculated by using Equations (12) and (16). The inductors with negative currents also discharge their energy in the capacitors. This energy is then transferred to the output capacitor. Thus the total energy can be written as:

$$\Delta ET = \frac{D^2 T^2}{2L} * (VR^2 + VY^2 + VB^2) \tag{17}$$

Which can be written as:

$$= \frac{3D^2 T^2}{4L}Vm^2 \tag{18}$$

The Equation (18) represents total energy input to the converter in DT time [4, 10]. It can be noted here that, the energy absorption is only happening for the DT time. As the Total time cycle is of T seconds. The input power can be written as:

$$P_{in} = \frac{\Delta ET}{T} \tag{19}$$

$$\Rightarrow P_{in} = \frac{3D^2 TVm^2}{4L} \tag{20}$$

$$\therefore P_{out} = \eta P_{in} \tag{21}$$

$$\Rightarrow P_{out} = \frac{V_o^2}{RL} \tag{22}$$

$$V_{out} = \sqrt{\eta P_{in} RL} \tag{23}$$

$$\Rightarrow V_o = \sqrt{\frac{3\eta T}{L}}\frac{DVm}{2} \tag{24}$$

3 | WIND TURBINE EMULATION

A separately excited DC motor is used for wind turbine emulation in this work. The armature current control method is used for generating the torque-speed characteristic of a wind turbine. In the developed system, a two-blade wind turbine (MOD2) is emulated, as these turbines have the maximum power coefficient (CP) at around tip speed ratio (λ) of 7. This value of lambda ensures voltage generation from the mechanically coupled SEIG. Figure 6 shows the schematic diagram of the developed system.

Mechanical power output of the turbine is:

$$Pm = \frac{1}{2}Cp\rho AW^3$$

Where, Cp is a well established function of λ and pitch angle (β). An approximate model of performance coefficient for MOD 2 wind turbine is given in [22] as a non-linear function given by:

$$Cp = C_1(C_2 - C_3 v - C_4 v^x - C_5)e^{-c_6(\lambda,\theta)}. \tag{25}$$

where,

$$C_1 = 0.5, \quad C_2 = 116/\lambda_i, \quad C_3 = 0.4$$
$$C_4 = 0, \quad C_5 = 5, \quad C_6 = 21/\lambda_i.$$

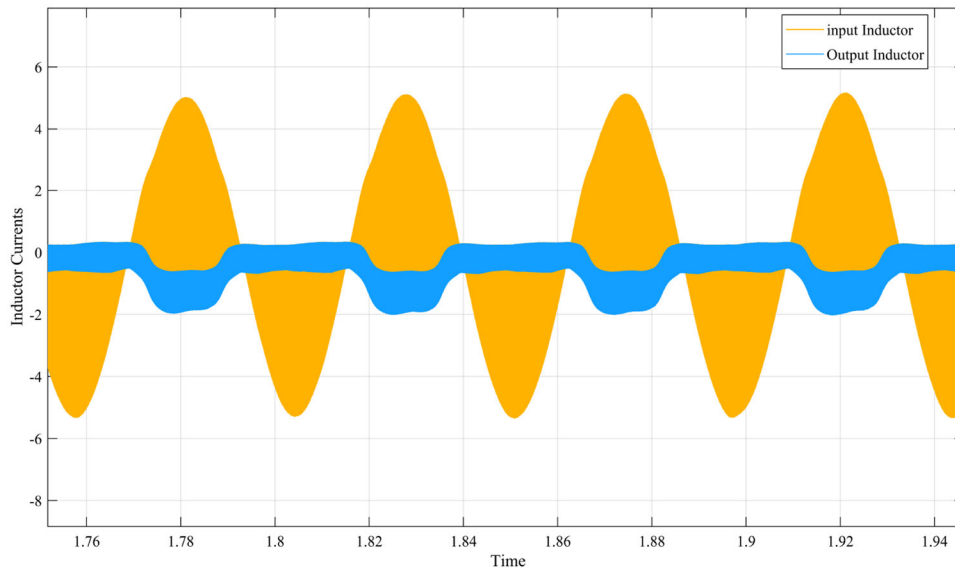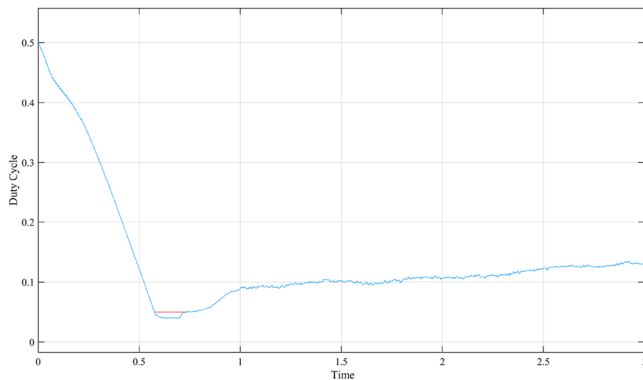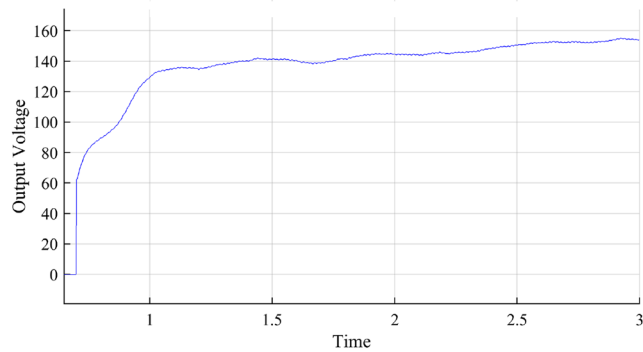$$\lambda_i = \frac{1}{\lambda + 0.08v} - \frac{0.035}{v^3 + 1}.$$

FIGURE 11   Current waveform of input and output inductors

(a) Duty variation for MPPT

(b) Output voltage of the converter

FIGURE 12   MPPT characteristics

3.1 | MPPT and control

The availability of wind energy is stochastic in nature. This necessitates implementation of an MPPT technique to decrease overall cost by maximizing utilization. Generally, MPPT tech-

niques in wind systems are based on the DC link voltage and current, or by measuring the blade speed and torque of the generator [18]. With miniaturization and mass production of voltage and current sensors, they are extensively being used for condition monitoring and system control.

In this paper, a unique MPPT technique is implemented by measuring the three-phase voltages and currents of the generator. Figure 7 shows a flowchart showing the MPPT technique used. As shown in Equation (12), a DC value proportional to three-phase current can be calculated. Using these proportional DC values of voltage and current of the generator, the duty cycle of the AC–DC converter can be adjusted accordingly to get maximum power. The Control of the emulator can be easily implemented by measuring the speed of the DC motor to generate a reference torque using Equation (25). The torque applied by the DC motor is calculated by multiplying the measured armature current by the torque constant. The DC motor torque is then controlled by using a PI controller. The assumed parameters for the turbine, and values of K_p and K_i, are given in Table 3.

4 | SIMULATION AND DISCUSSION

The simulation of the proposed converter is done in Matlab Simulink 9.0 as per the parameters given in Tables 2 and 3. The system performance on the basis of the input voltage, MPPT technique, output voltage, inductor current, and switching stress is done. It is evident from the Figures 8 and 9 that the proposed system is working as per the design considerations.

Figure 9 shows the voltage and current at the input side of the filter. A low pass LC filter is used in this circuit, with inductors of 560 μH and AC capacitors of 10 μF. As the circuit is connected with the generator at 0.7 s, current waveforms exhibits the transients as the LC filter is energized. The MPPT technique
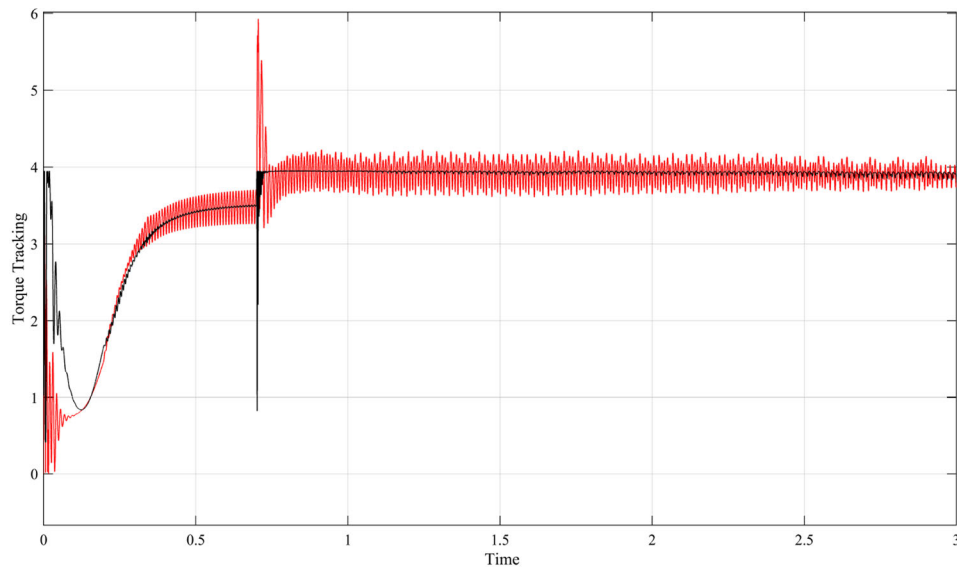
(a) Tracking of the generated reference torque
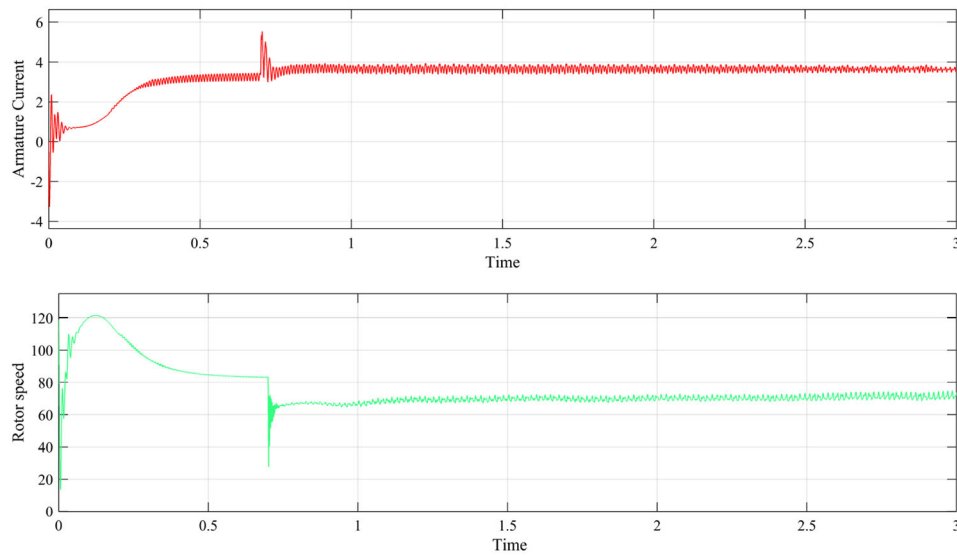
(b) Armature current(A) and speed(rad/s) of the turbine emulator

FIGURE 13 Wind turbine emulator response

TABLE 4 Component Specification

Component	Attributes	Nos
MOSFET	650 V, 65 A	3
Diode	ULTRAFAST, 1KV, 65 A	3
Optocoupler	FOD3184, 3 A	3
DC Film Capacitor	1 μF 1.2 KV	3
Electrolytic capacitor	1000 μF, 600 V	1
Inductor	47 μH	3
Inductor	560 μ H	3

is dependent on the calculated values of the voltage and current maxima. These values are shows in Figure 10.

The input inductor is working in deep DICM, and the calculated voltage and current maxima values are DC in nature. The output inductor is intended to work in the CICM for output DC voltage to have low ripples. Figure 11 shows that the output inductor current is in CICM around the maxima and in DICM around zero crossing of the input voltage. This drawback is compensated by the 120 deg phase-shifted output currents in the three output inductors, which results in lower output voltage ripple.
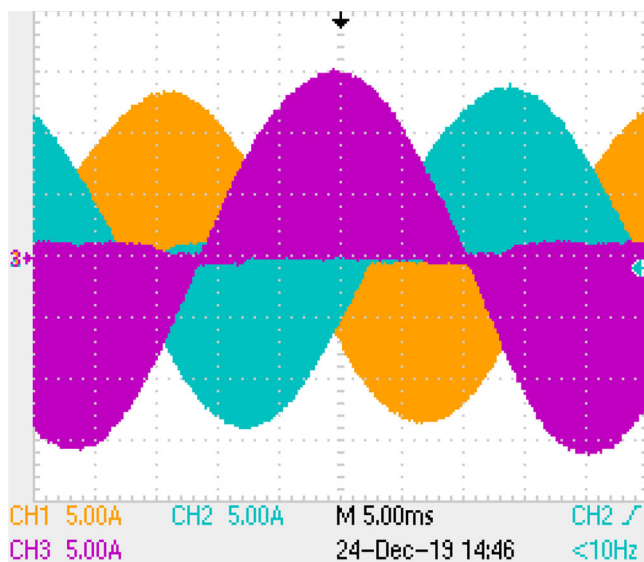
FIGURE 14 Input inductor current waveform (I_{peak}=15 A). Current in R phase (channel-3 at 5 A/div), Y phase (channel-1 at 5 A/div), B phase (channel-2 at 5 A/div)
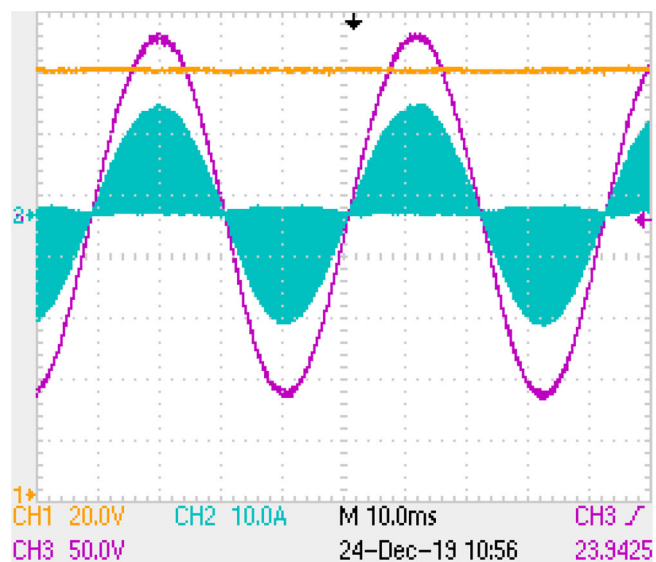

FIGURE 16 Voltage of R phase (channel-3 at 50 V/div) and input current (channel-2 at 10 A/div) and output voltage of the converter (channel-1 at 20 V/div)
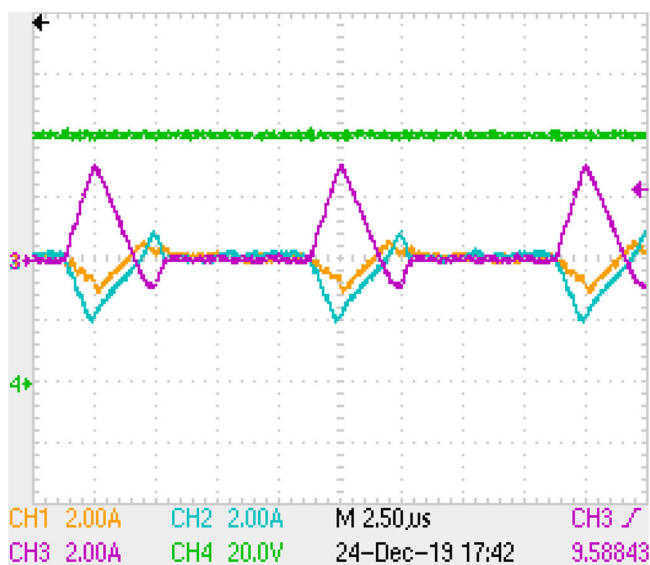

FIGURE 15 Current waveforms at 10% duty. Current in R phase (channel-3 at 2 A/div), Y phase (channel-1 at 2 A/div), B phase (channel-2 at 2 A/div) and output voltage on channel-4 at 20 V/div

FIGURE 17 Generator voltage (channel-1 at 50 V/div) and current (channel-2 at 2 A/div) with output voltage of converter (channel-4 at 20 V/div)

Figure 12a shows the variation of the duty as per the methodology shown in Figure 7; the generator is connected with the converter at 0.7 s. In the simulations, a system consisting of DC motor based wind emulator and SEIG is considered, which increases the overall settling time. The MPPT technique is found to be robust enough to respond satisfactorily. The variation of the output voltage with duty variation is shown in Figure 12b.

Figure 13 shows the tracking of the reference torque by the DC motor. The higher value of Ki ensures stable operation of the controller with high ripple current drawn by the DC motor.
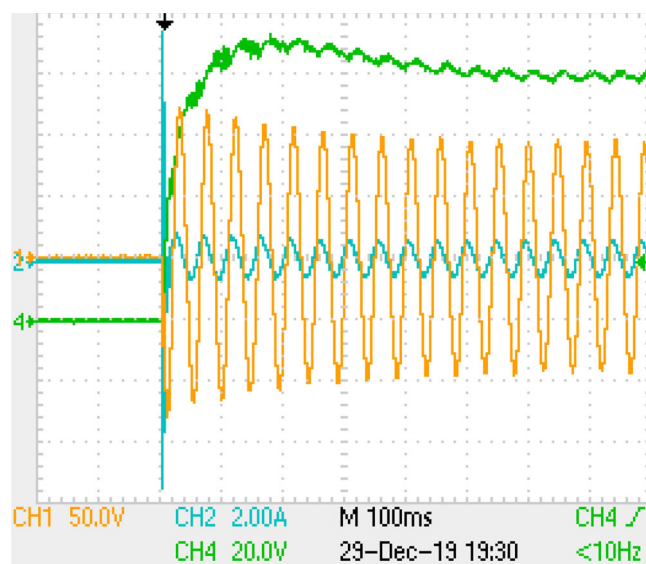
In Figure 12b the simulated current and speed waveform off the DC motor is shown. The sudden decrease in the speed is due to loading of the SEIG at 0.7 s. After loading the generator, MPPT technique controls the converter duty and the emulation logic controls the current from the buck converter in order to follow the intended torque–speed characteristic of the wind turbine.
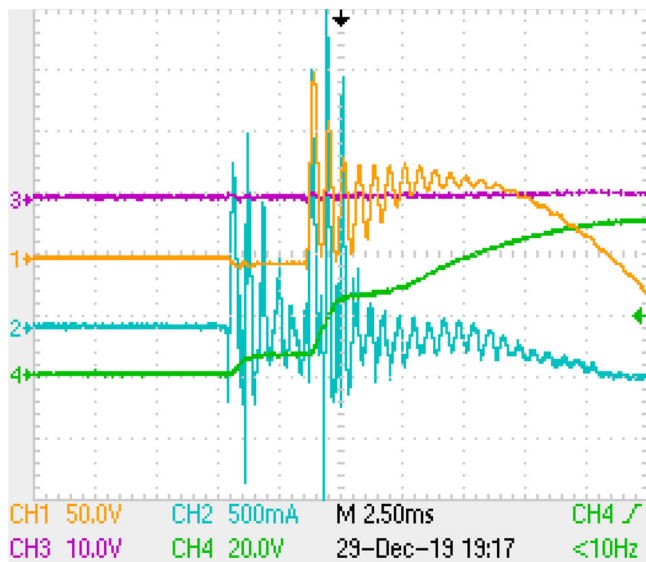
FIGURE 18 Transient filter voltage (channel-1 at 50 V/div) and current (channel-2 at 500 mA/div) waveforms and output voltage(channel-4 at 20 V/div)
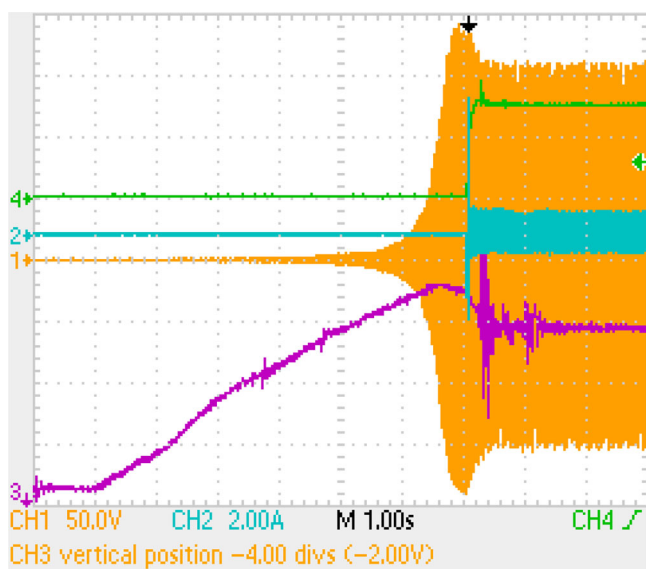

FIGURE 20 Experimental setup

FIGURE 19 SEIG voltage buildup (channel-1 at 50 V/div), generator current (channel-2 at 2A/div), speed of SEIG (channel-3 at 200 RPM/div) and output voltage (channel-4 at 100 V/div)

5 | HARDWARE RESULTS AND DISCUSSION

DSpace-CP1104 is used to develop the hardware prototype for this work. NTHL040N65S3F MOSFET transistor is used for switching with FOD3184 optocoupler. The details of the components used are given in Table 4.

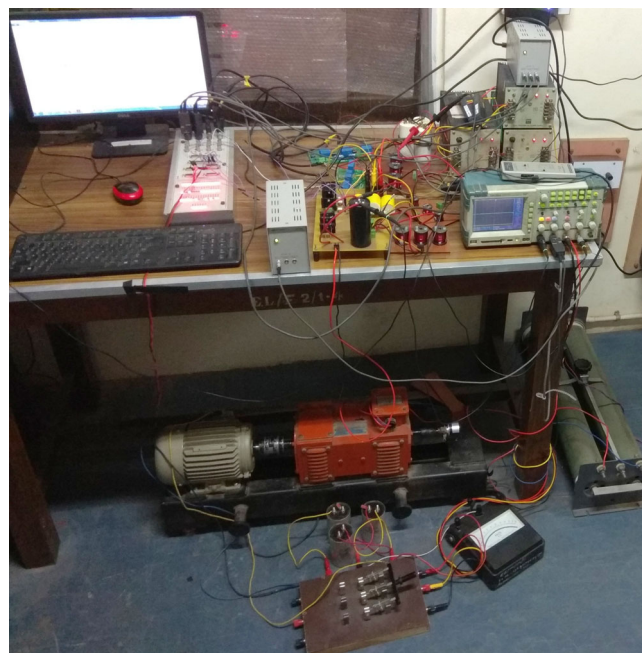Figure 14 shows the input current waveforms of the converter under loaded condition. The input inductor currents in phases having negative voltages are also in the negative direction as the input inductors are working in DICM. An instance of current waveform is shown in Figure 15, where phase A has a positive voltage and thus has positive current (channel-3), while the other two phases carry negative currents (channel-1 and 2), and output voltage on channel-4 is constant.

The PFC in the proposed converter is shown in the Figures 8 and 16, the per phase voltages and currents are found to be in phase. The high frequency switching of the input current can be easily filtered by a small LC lowpass filter.

Figure 17 shows variation of the voltage and current drawn from the SEIG (channels-1 and 2), and the output voltage on channel-4. The transients in voltage and current on connection of the converter to the generator is shown in Figure 18. It can be observed that the transient phase passes in under 15 ms.

In Figure 19, the voltage build-up of the SEIG is shown. A change in generated voltage (channel-1) is observed on connecting the converter to the generator, which is marked by an increase in the output voltage (channel-4) and generator current (channel-2). The speed is measured by an optical encoder and then converted to analog signal using a DAC (1 V/400 RPM), which is shown on channel-3.

6 | CONCLUSION

A new three-phase bridgeless cùk converter is proposed, analyzed, and validated in this work. The proposed single-stage converter is found suitable for three-phase generators as it eliminates front-end DBR. The DICM operation of input inductor ensures lesser switching stress and inherent PFC. The wide

range of output voltage control of the cùk converter leads to better MPPT technique implementation. An MPPT control based on three-phase voltages and currents is also reported, which eliminates the need for an intermediate DC stage. The satisfactory results obtained from the SEIG based wind generation is indicative of the suitability of the converter's application in standalone WECS.

ORCID

Kalpana Chaudhary 🔟 https://orcid.org/0000-0003-3393-2093

REFERENCES

1. World Bank: Toward a Sustainable Energy Future for All. World Bank Group's Energy Sector (2013). https://www.worldbank.org/content/dam/Worldbank/document/SDN/energy-2013-0281-2.pdf
2. Lo, K.Y., et al.: MPPT battery charger for stand-alone wind power system. IEEE Trans. Power Electron. 26(6), 1631–1638 (2011). https://www.ti.com/lit/ug/tidue54b/tidue54b.pdf?
3. Texas Instruments: 98.6% Efficiency, 6.6-kW Totem-Pole PFC Reference Design for HEV/EV Onboard Charger. TI Designs, TIDA-01604 1–72 (2018).
4. Ismail, E.H.: Bridgeless SEPIC rectifier with unity power factor and reduced conduction losses. IEEE Trans. Ind. Electron. 56(4), 1147–1157 (2009)
5. Bist, V., Singh, B.: A unity power factor bridgeless isolated Cuk converter-fed brushless DC motor drive. IEEE Trans. Ind. Electron. 62(7), 4118–4129 (2015)
6. Sabzali, A.J., et al.: New bridgeless DCM sepic and Cuk PFC rectifiers with low conduction and switching losses. IEEE Trans. Ind. Appl. 47(2), 873–881 (2011)
7. Anand, A., Singh, B.: Cuk-SEPIC based bridgeless PFC dual output converter fed SRM drive. India International Conference on Power Electronics, IICPE 2018, 1–7 (2018)
8. Fardoun, A.A., et al.: New efficient bridgeless Cuk rectifiers for PFC applications. IEEE Trans. Power Electron. 27(7), 3292–3301 (2012)
9. Lee, S.W., Do, H.L.: Single-stage bridgeless AC–DC PFC converter using a lossless passive snubber and valley switching. IEEE Trans. Ind. Electron. 63(10), 6055–6063 (2016)
10. Singh, B., Bist, V.: Improved power quality bridgeless Cuk converter fed brushless DC motor drive for air conditioning system. IET Power Electron. 6(5), 902–913 (2013)
11. Yang, H.T., et al.: Implementation of bridgeless Cuk power factor corrector with positive output voltage. IEEE Trans. Ind. Appl. 51(4), 3325–3333 (2015)
12. Lin, X., Wang, F.: AC–DC bridgeless buck converter with high PFC performance by inherently reduced dead zones. IET Power Electron. 11(9), 1–7 (2018)
13. Su, B., Lu, Z.: An interleaved totem-pole boost bridgeless rectifier with reduced reverse-recovery problems for power factor correction. IEEE Trans. Power Electron. 25(6), 1406–1415 (2010)
14. Tang, Y., Khaligh, A.: A multiinput bridgeless resonant AC-DC converter for electromagnetic energy harvesting. IEEE Trans. Power Electron. 31(3), 2254–2263 (2016)
15. Wu, H., et al.: Three-port bridgeless PFC-based quasi single-stage single-phase AC–DC converters for wide voltage range applications. IEEE Trans. Ind. Electron. 65(7), 5518–5528 (2018)
16. Jimichi, T., et al.: Comparison of single-phase and three-phase dual-active bridge DC–DC converters with various semiconductor devices for off-shore wind turbines. 2017 IEEE 3rd International Future Energy Electronics Conference and ECCE Asia, pp. 591–596. IEEE, Piscataway, NJ (2017)
17. Tan, K., Islam, S.: Optimum control strategies in energy conversion of PMSG wind turbine system without mechanical sensors. IEEE Trans. Energy Convers. 19(2), 392–399 (2004)
18. Abo.Khalil, A.G., Lee, D.C.: MPPT control of wind generation systems based on estimated wind speed using SVR. IEEE Trans. Ind. Electron. 55(3), 1489–1490 (2008)
19. Kalla, U.K., et al.: Adaptive sliding mode control of standalone single-phase microgrid using hydro, wind, and solar PV array-based generation. IEEE Trans. Smart Grid 9(6), 6806–6814 (2018)
20. Wang, H., Blaabjerg, F.: Reliability of capacitors for DC-link applications in power electronic converters - An overview. IEEE Trans. Ind. Appl. 50(5), 3569–3578 (2014)
21. Gu, L., et al.: Means of eliminating electrolytic capacitor in ac/dc power supplies for led lightings. IEEE Trans. Power Electron. 24(5), 1399–1408 (2009)
22. Han, Y.H.: Grid Integration of Wind Energy Conversion Systems. Vol. 21. Wiley, Weinheim (2000)